IRANIAN JOURNAL OF CATALYSIS

Nano cotton-shape mesoporous (NCSM) modified by Fe₃O₄: Green, magnetic and reusable catalytic system for dechlorization of bromothymol blue (BTB)

Hamid Aliyan*

Department of Chemistry, Shahreza Branch, Islamic Azad University, 86145-311, Iran.

ABSTRACT

Fe₃O₄-containing cotton-like mesoporous silica system (Fe₃O₄@NCSM) was studied with regard to its performance towards the photodecolorization of bromothymol blue (BTB) aqueous solution. The surface properties of the functionalized catalyst were analyzed by a series of characterization techniques like FTIR, XRD, BET, SEM and TEM. The N₂ Adsorption–desorption analysis shows that the mesostructure of silica remains intact after Fe₃O₄ modifications, while the spectral technique shows the successful encapsulating of the neat Fe₃O₄ inside the porous silica support. The optimum values of the experimental parameters which affect the degradation efficiency were obtained as: 0.15 g L^{-1} of the photocatalyst, 25 ppm dye concentration and pH 5.6.

Keywords: Nano cotton-shape mesoporous (NCSM), Fe₃O₄; Heterogeneous photocatalysis, Bromothymol blue (BTB).

1. Introduction

Environmental pollution has increased more and more public concern nowadays [1]. Due to daily increase of industrial units, pollution of water resources by industrial effluents is hazardous for human and environmental health. Most of dyes, as one of the most common groups of water pollutants, have very low biological capability analysis and some of them are hazardous to marine biological activity. Presence of dyes even less than 1 mg L^{-1} is important from a visible appearance point of view [2,3]. Heterogeneous photodegradation processes involving metal-oxide semiconductors have been widely used for photocatalytic environmental remediation especially wastewater decontamination, due to high photosensitivity, nontoxic nature, low cost and environment friendly features [4–13]. It is well known that the size, morphology, and structure of mesoporous materials significantly influence their physical and chemical properties and, therefore, their applications [14]. Recently, much effort has been devoted to developing novel approaches for tailoring the structure of mesoporous materials to have specific morphologies, which is an important goal of material scientists. Studies have shown that combinations of various micelles interactions have led to the development of helical rods and fibers [15,16], shells [17], faceted rhombododecahedrons [18] and hollow spheres, and solid or leaf-shaped spheres [19,20]. Based on this idea, a series of mesoporous materials with special morphologies, including solid spheres, hollow spheres and leaf-shaped has been synthesized using different dual-template combinations [21-23].

Herein, we focus our attention on the effects of the pore topology on the state of supported Fe₃O₄ species on Nano Cotton-like mesoporous (NCSM) by the encapsulation method. In addition to a complete characterization of supported catalyst, this photocatalytic performance is shown for photodegradation of bromothymol blue (BTB) aqueous solution. BTB with the molecular formula of $C_{27}H_{28}Br_2O_5S$ was used as a dye for painting plant tissue (cell wall and nucleus) and in fish breathing tanks to determine the amount of carbonic acid. BTB stimulates the respiratory, digestive, skin and eye diseases [24,25].

*Corresponding author email: aliyan@iaush.ac.ir
Tel.: +98 31 5329 2515; Fax: +98 31 5351 3103

2. Experimental

2.1. General information

All materials were commercial reagent grade. Infrared spectra (400–4000 cm^{-1}) were recorded from KBr pellets on a PerkinElmer Spectrum 65 spectrometer. The X-ray powdered diffraction patterns were performed on a Bruker-D8ADVANCE with automatic control. The patterns were run with monochromatic Cu Kα (1.5406 Å) radiation with a scan rate of 2° min^{-1}. Nitrogen adsorption measurements were performed at −196 ∘C by using an ASAP 2010M surface analyzer, and the pretreatment temperature was 180°C. Transmission electron micrographs (TEM) were obtained on a Joel JEM 2010 scan-transmission electron microscope. The sample for the TEM measurement was suspended in ethanol and supported on a carbon coated copper grid. The morphologies of samples were also investigated using a Philips, XL30 scanning electron microscope (SEM) with an accelerating voltage of 17 kV. The BET method was employed to measure the surface area of NCSM samples with a Micromeritics Gemini 2360 surface area analyzer.

2.2. Preparation of the catalysts

2.2.1. Preparation of NCLM

Pluronic F127 (Pluronic F127 is a difunctional block copolymer surfactant terminating in primary hydroxyl groups, which has a triblock PEO−PPO−PEO structure (PEO: poly(ethylene oxide); PPO: poly(propylene oxide)) (0.5 g) was dissolved in a mixture of ethanol (20 mL) and water (80 mL) under stirring for 30 min. Dodecylamine, DDA (1.17 g) and Tetraethyl orthosilicate (TEOS is mainly used as a crosslinking agent) (5 mL) were then added into the solution and the mixture was stirred for 24 h at room temperature. The solid product was recovered by filtration, then dried and extracted or calcined [26].

2.2.2. Preparation of Fe$_3$O$_4$@NCSM

Mixing 50 mg of Fe$_3$O$_4$ and 100 mg of the NCSM sample with 10 mL of distilled water was added to the Teflon container with the rest of the mixture under static conditions at 493 K for 8 h. According to elemental analysis, the loadings were obtained 27 wt%.

2.3. The catalytic activity

In order to study the photodegradation of BTB, a photo-catalytic reactor system constructed cylindrical Pyrex-glass cells was used. The photocatalytic removal of BTB from aqueous solution was studied by suspending an optimized amount of Fe3O4@NCSM

powder (0.1 g L^{-1}) in 4 mg L^{-1} of BTB aqueous solution (with initial pH of 7.8). The blank solution had the same conditions of analyte without the photocatalyst. The suspensions were irradiated using a Hg lamp (35W, G-line, blue, maximum intensity at 435.5 nm) and at definite time intervals, the suspensions were centrifuged for 10 min and the absorbance of the cleaned samples was measured at 616 nm (at the optimized conditions) by using a calibrated UV–vis spectrophotometer (Carry 100 Scan). As illustrated in Section 3.2.3, by varying the pH of solutions the corresponding maximum absorption wavelengths changed and the solution absorbencies were recorded at the corresponding wavelengths. The degradation percentage of BTB was estimated by applying the following equation using blank (A$_0$) and sample (A) absorbance:

$$Degradation\% = 100\ (A_0\text{-}A)\ /A_0$$

To remove the surface adsorption effect, before irradiation experiments the suspension was stirred for 40 min to reach equilibrium adsorption–desorption phenomena. The following first kinetics model was also used for calculation of rate constants (k) [27]:

$$\ln(C_t/C_0) = -kt$$

3. Results and Discussion

3.1. Physico-chemical characterization

Fig. 1 presents the FTIR spectra in the skeletal region of 4000–400 cm^{-1} for the Fe$_3$O$_4$@NCSM. The typical bands due to siliceous Si–O–Si material are observed: A main band at 1077 and 1201 cm^{-1}, due to asymmetric Si–O–Si stretching modes. The symmetric stretching modes of Si–O–Si groups are observed at around 809 cm^{-1}. [28]. The peak at 968 cm^{-1} is assigned to defective Si–OH groups. The peak at 561 cm^{-1} could be attributed to the Fe-O stretching of Fe$_3$O$_4$ [29].

XRD patterns of parent NCSM and Fe3O4@NCSM at low angle region (2θ = 1-10°) are shown in Fig. 2a. The main diffraction peaks appear at 2θ = 3.93 and 2θ= 4.02 for NCSM and Fe3O4@NCSM, respectively.
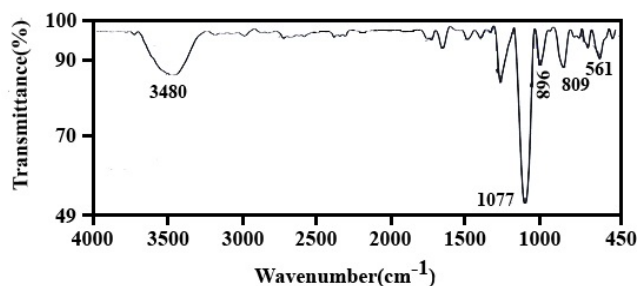
Fig. 1. FTIR spectra for the Fe$_3$O$_4$@NCSM.
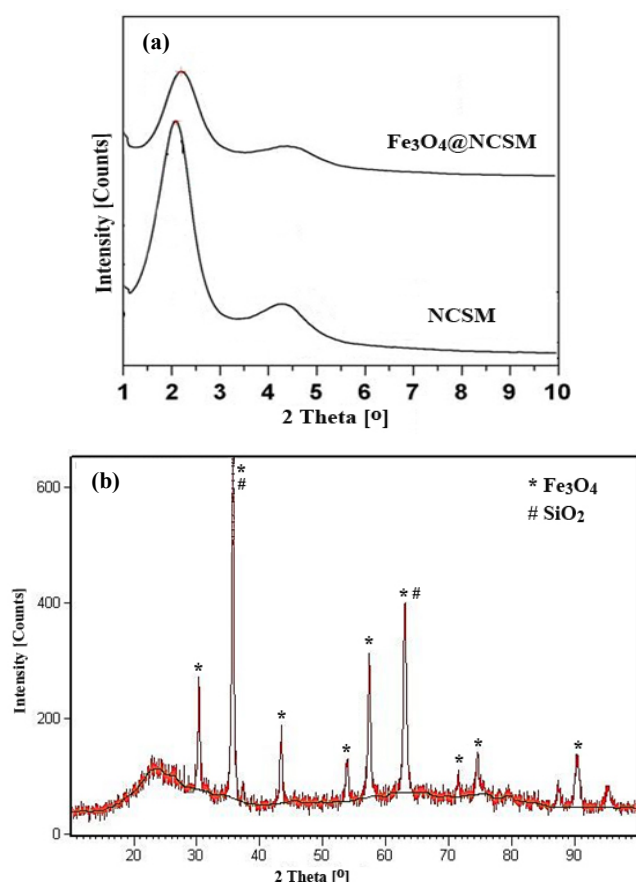
Fig. 2. XRD patterns of NCSM and Fe₃O₄@NCSM (a) 2θ=1-10º; (b) 2θ=10-100º.

A slight shift of the primary peak occurs at higher *2θ* values after impregnation. In addition, the decreased intensities of the reflections indicate that the adopted synthesis procedure yields less ordered materials, a partial structural collapse of the pores and decreased electron density contrast compared to traditional NCSM, as previously observed in V/SBA [30] V/MIL-101 [31] and V/MCF [32] and V/RSM [33] systems.

Fig. 2b shows XRD patterns of Fe₃O₄@NCSM at region (2θ = 10-100º). The XRD patterns of magnetic Fe₃O₄ nanoparticles reveal that the crystal structure is indexed as face-centered cubic (fcc) (JCPDS card No. 19-629). No other characteristic peaks due to the impurities of hematite or hydroxides were detected. It was found that the strong diffraction peaks were situated at 2θ of 18.90, 30.220, 35.530, 43.240, 53.970, 57.440, and 62.940, corresponding to the diffractions of [111], [220], [311], [400], [422], [511], and [440] crystal faces of porous Fe₃O₄ structures, respectively. Sharp peaks in Fig. 3 suggest that the Fe₃O₄ nanoparticles have good crystalline abilities [29].

The TEM images of Fe₃O₄@NCSM sample is shown in Fig. 3. The synthesized cotton-like mesoporous material clearly displayed a cotton shape and worm-like porous structure [26]. The same morphology was obtained for Fe₃O₄@NCSM. TEM analyses indicate that the wrinkles porous structure of the NCSM is robust enough to survive the Fe₃O₄ incorporation process and so offers an excellent matrix to support highly dispersed Fe₃O₄ species.
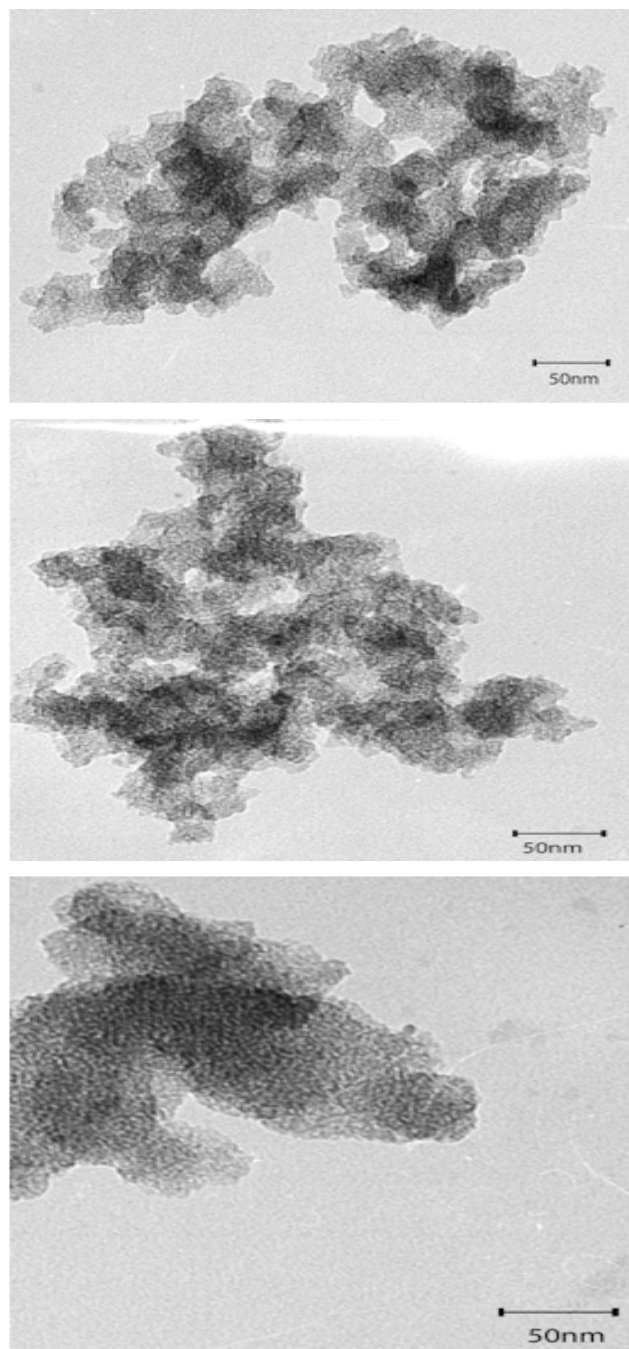

Fig. 3. TEM images of Fe₃O₄@NCSM.

The SEM images of NCSM and Fe_3O_4@NCSM particles are shown in Figs. 4a and 4c, respectively. NCSM and Fe_3O_4@NCSM exhibited nearly the dense aggregate of cotton-shape morphology. There is no definite shape shown for any particles. The NCSM and Fe_3O_4@NCSM particles have been found to have high purity by EDX measurements (Figs. 4b and 4d). EDX results indicated that the Fe_3O_4@NCSM samples contain Fe, Si and O elements.

Fig. 5 shows N_2 adsorption-desorption isotherms and pore size distributions of NCSM and Fe_3O_4@NCSM, which are similar to those of NCSM. As typically observed in mesoporous materials, both samples show typical IV type isotherms and H1 type hysteresis looped at high relative pressures according to the IUPAC nomenclature [34], which are the typical characteristics of mesoporous materials [35].

Structural properties of NCSM are listed in Table 1. NCSM showed BET surface area of 1035 m^2/g and pore volume of 1.14 cm^3/g. After Fe_3O_4 modification, the nitrogen adsorption isotherm (Fig 5a) became an even line and the volume adsorbed decreased distinctly, suggesting the occupation of the pore by Fe_3O_4. BET surface area and pore volume of Fe_3O_4@NCSM samples decreased, which confirms that Fe_3O_4 have occupied the channels in NCSM.

(a)

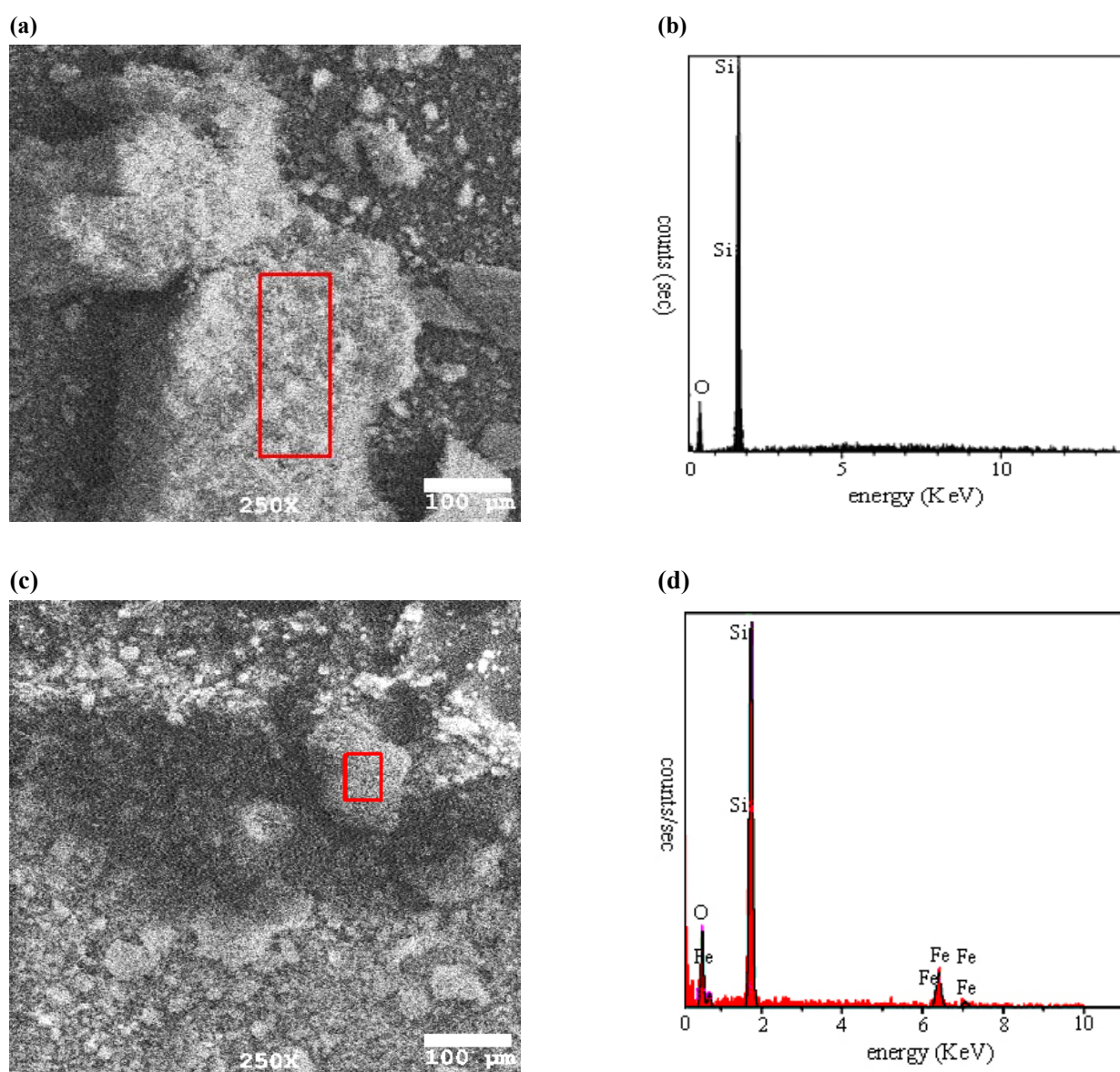**(b)**

(c)

(d)

Fig. 4. (a,c) SEM images for NCSM and Fe_3O_4@NSCM and (b,d) EDS measurements carried out during SEM observations for NCSM and Fe_3O_4@NCSM, respectively.

Table 1. The texture parameters of NCSM and Fe$_3$O$_4$@NCSM samples.

Materials	Texture parameters (N$_2$ adsorption)		
	Surface area (m^2/g)	Pore volume (cm^3/g)^{a,b}	Pore diameter (nm)
CLM	1035	1.14	4.40
Fe$_3$O$_4$@CLM	662	0.84	5.08

^{a}Total pore volume measured at p/p$_0$ = 0.99.
^{b}Pore volume and pore size (by BJH method) were determined from N$_2$ adsorption at 77K.

3.2. Photocatalytic activity

3.2.1. Effect of catalyst weight

The effect of the amount of Fe$_3$O$_4$@NCSM catalyst on the photodegradation of BTB was studied in the range of 0.05–0.25 g L^{-1} and the obtained results are presented in Fig. 6a. The rate constant values, k (min^{-1}), were also calculated from the straight-line segment of the corresponding first-order plots as a function of the catalyst mass and the results are listed in Table 2.
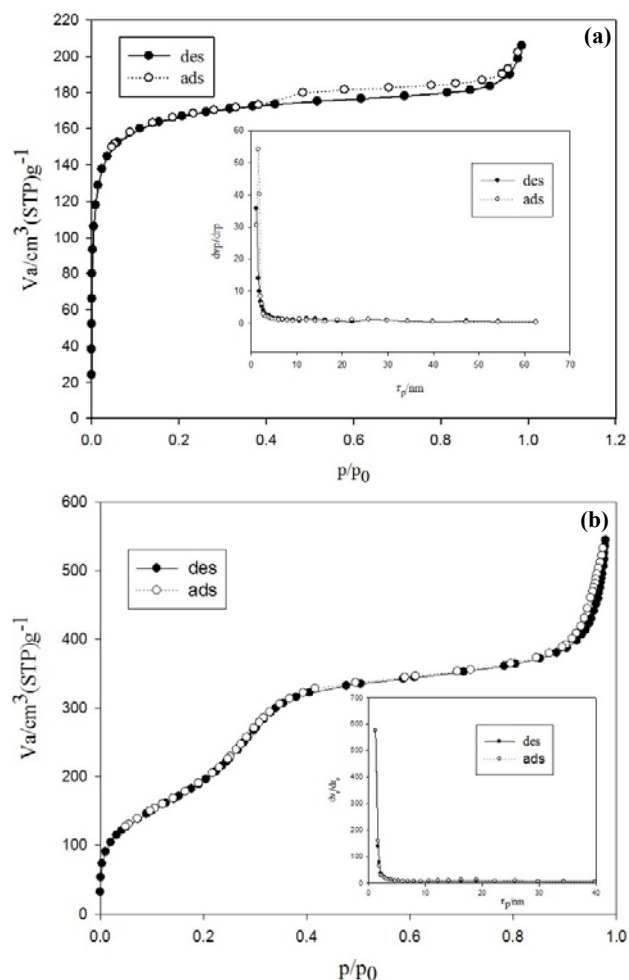

Fig. 5. N$_2$-adsorption-desorption isotherms of (a) NCSM and (b) Fe$_3$O$_4$@NCSM: (inset) pore size distributions calculated by the BJH method.
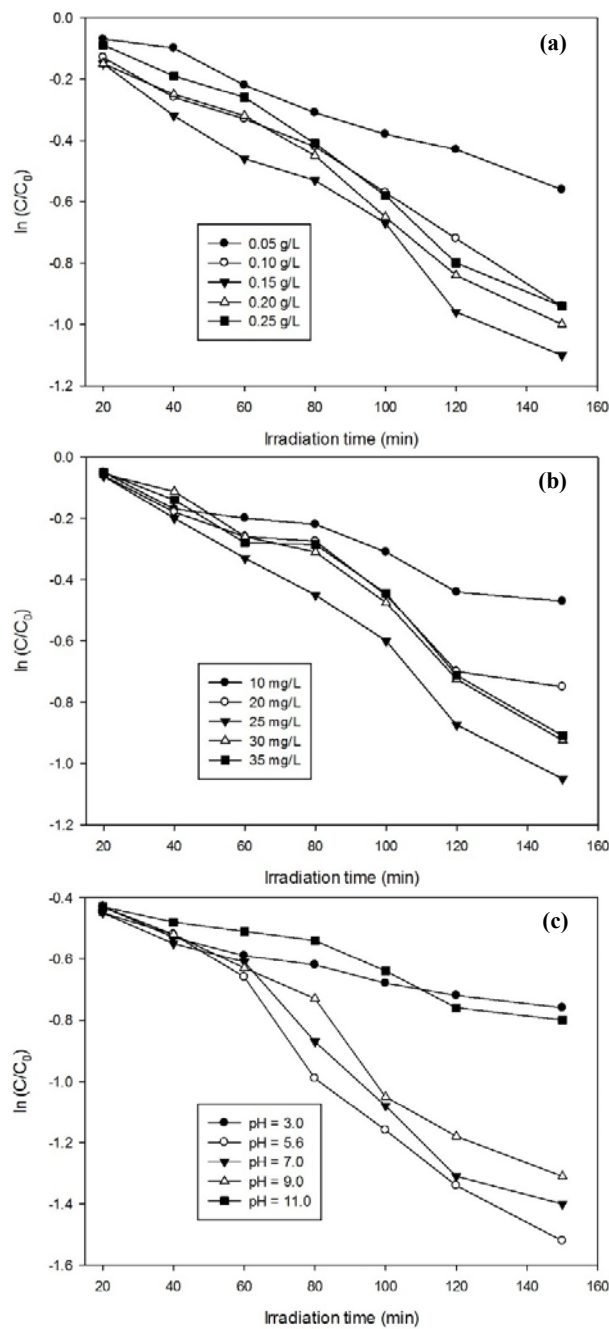

Fig. 6. Effect of (a) Fe$_3$O$_4$@NCSM dosage on decolorization efficiency; (b) initial dye concentration of BTB on the decolorization efficiency and (c) solution pH on the BTB dye decolorization.

Table 2. Rate constants as a function of experimental parameters.

Parameter	Value	$k \times 1000$ (min^{-1})
Amount of the photocatalyst (g L^{-1})	0.05	1.75
	0.10	1.98
	0.15	2.02
	0.20	1.76
	0.25	1.32
pH	3.2	1.37
	5.6	2.31
	7.0	1.72
	9.0	1.54
	11.0	1.08
C_{BTB} (mg L^{-1})	10	1.12
	20	1.73
	25	2.15
	30	2.01
	35	1.86

The initial rates of the degradation increased with increasing in the weight of the catalyst up to an optimum loading of Fe$_3$O$_4$@NCSM (0.15 g L^{-1}) and further increasing had a negative effect. Increasing in the weight of the catalyst (or increasing in number of Fe$_3$O$_4$@NCSM particles), increases the numbers of adsorbed BTB molecules onto the catalyst surface. So the rate was enhanced. The decrease in the initial rate beyond the catalyst dosage of 0.15 g L^{-1} may be attributed to the screening effect of excess catalyst particles in the solution which decreases the light penetration and hence reduces the photodegradation rate [36]. Another reason is aggregation of solid particles while large amount of catalyst was used [37,38]. Hence, adequate dosage of the catalyst increases the generation rate of electron/hole pairs; thus, the formation of OH radicals for enhancing photodegradation.

3.2.2. Effect of the initial BTB concentration

The photocatalytic degradation of BTB was investigated at different initial concentrations covering the range from 10 to 35 ppm and the results are collected graphically in Fig. 6b. By increasing the initial concentration, a bigger quantity of BTB molecules was adsorbed on the surface of the Fe$_3$O$_4$@NCSM catalyst, and therefore, the generation

of hydroxyl radicals would be reduced since there were fewer active sites for the adsorption of hydroxyl ions. Further, at higher concentration of BTB in the solution, the photons would be able to be absorbed by the BTB molecules before they could reach the catalyst surface. This in turn reduces absorption of photons by the catalyst and, consequently, the degradation efficiency [29].

3.2.3. Influence of pH on the degradation efficiency

Bromthymol Blue is a dye used as an indicator in determining pH. Bromthymol blue is a weak acid. It can be in acid or base form, depending on the pH of the solution.

The pH of the solution affects the photodegradation processes due to the strongly pH dependent properties such as semiconductor's surface charge state, flat band potential, and dissociation of compounds in the solution. So, the effect of pH was investigated on the efficiency of the photodegradation process under optimal conditions in the pH range of 3.0–11 and the results are collected in Fig. 6c and Table 2.

Fig. 6c shows the plot of ln(C0/C) versus time as a function of the pH of BTB solution. The rate constant values (k, min−1) as a function of pH on the degradation process are presented in Table 2. As it shows, the rate of degradation increases with an increase in pH of up to 5.6 and then it decreases.

The pH of the point of zero charge (pH$_{pzc}$) for Fe$_3$O$_4$@NCSM has been calculated by different methods and reported near 4.5-5.0 [29]. The charge of the catalyst surface is positive and negative at pH values smaller and higher than the pH$_{pzc}$, respectively. The adsorption of BTB as weak acid is quite good at pH near the pzc of photocatalyst, and hence, higher BTB photodegradation efficiency was expected at pH of 5.6. This result suggests that weak acidic and circumneutral initial pH favored dye photodegradation.

4. Conclusion

Based on the results, Fe$_3$O$_4$@NCSM as catalyst prepared by encapsulated method, significantly increased its efficiency in the photodecolorization of the BTB dye. The observations of these investigations clearly demonstrated the importance of choosing the optimum degradation parameters such as pH, concentration and dosage of the catalyst in obtaining a high degradation rate.

Acknowledgements

References

[1] X. Hui-Li, Z. Hui-Sheng, Z. Tao, X. Dong-Chang, J. Environ. Sci. 19 (2007) 1141-1145.

[2] C. Sahoo, A.K. Jupta, A. Pal, Desalination 181 (2005) 91–100.

[3] S. Senthilvelan, V.L. Chandraboss, B. Karthikeyan, L. Natanapatham, M. Murugavelu, Mater. Sci. Semicond. Process 16 (2013) 185–192.

[4] A. Saepurahman, M.A. Abdullah, F.K. Chong, Chem. Eng. J. 158 (2010) 418-425.

[5] Zh. Aiyong, Zh. Minghua, H. Lu, Zh. Qixing, Appl. Catal. A 385 (2010) 114-122.

[6] S. Chin, E. Park, M. Kim, J. Jurng, Powder Technol. 201 (2010) 171-176.

[7] H. Faghihian, A. Bahranifard, Iran. J. Catal. 1 (2011) 45-50.

[8] H.R. Pouretedal, M. Ahmadi, Iran. J. Catal. 3 (2013) 149-155.

[9] A. Nezamzadeh-Ejhieh, Z. Banan, Iran. J. Catal. 2 (2012) 79-83.

[10] A. Bagheri Ghomi, V. Ashayeri, Iran. J. Catal. 3 (2012) 135-140.

[11] A. Nezamzadeh-Ejhieh, M. Khorsandi, Iran. J. Catal. 1 (2011) 99-104.

[12] M.H. Habibi, E. Askari, Iran. J. Catal. 1 (2011) 41-44.

[13] H.R. Pouretedal; S. Basati, Iran. J. Catal. 2 (2012) 51-55.

[14] H.L. Xu, W.Z. Wang, Angew. Chem. Int. Ed. 46 (2007) 1489-1492.

[15] S. Yang, L.Z. Zhao, C.Z. Yu, X.F. Zhou, J.W. Tang, P. Yuan, D.Y. Chen, J. Am. Chem. Soc. 128 (2006) 10460-10466.

[16] G.L. Lin, Y.H. Tasi, H.P. Lin, C.Y. Tang, C.Y. Lin, Langmuir 23 (2007) 4115-4119.

[17] Y.Q. Yeh, B.C. Chen, H.P. Lin, C.Y. Tang, Langmuir 22 (2006) 6-9.

[18] B.C. Chen, M.C. Chao, H.P. Lin, C.Y. Mou, Microporous Mesoporous Mater. 81 (2005) 241-249.

[19] H. Blas, M. Save, P. Pasetto, C. Boissiere, C. Sanchez, B. Charleux, Langmuir 24 (2008) 13132-13137.

[20] Feng Z, Li YS, Niu DC, Li L, Zhao WR, Chen HR, Lei L, Gao JH, 295 Ruan ML, Shi JL., Chem. Commun. (2008) 2629-2631.

[21] J.G. Wang, F. Li, H.J. Zhou, P.C. Sun, D.T. Ding, T.H. Chen, Chem. Mater. 21 (2009) 612-620.

[22] H. Blas, M. Save, P. Pasetto, C. Boissiere, C. Sanchez, B. Charleux, Langmuir 24 (2008) 13132-13137.

[23] Z. Feng, Y.S. Li, D.C. Niu, L. Li, W.R. Zhao, H.R. Chen, L. Lei, J.H. Gao, M.L. Ruan, J.L. Shi, Chem. Commun. (2008) 2629-2631.

[24] E. Bishop, Indicators, Pergamon Press, New York, 1972.

[25] J.B. Puschett, B.S. Rao, B.M. Karandikar, K. Matyiaszewsui, Talanta 38 (1999) 335–338.

[26] L. Du, H. Song, S. Liao, Appl. Surf. Sci. 255 (2009) 9365–9370.

[27] N. Sobana, B. Krishnakumar, M. Swaminathan, Mater. Sci. Semicond. Process 16 (2013) 1046–1051.

[28] Z. Feng, Y.S. Li, D.C. Niu, L. Li, W.R. Zhao, H.R. Chen, L. Lei, J.H. Gao, M.L. Ruan, J.L. Shi, Chem. Commun. (2008) 2629-2631.

[29] H. Aliyan, R. Fazaeli, R. Jalilian, Appl. Surf. Sci. 276 (2013) 147-153.

[30] Y.M. Liu, Y. Cao, K.K. Zhu, S.R. Yan, W.L. Dai, H.Y. He, K.N. Fan, J. Catal. 224 (2004) 417-428.

[31] R. Fazaeli, H. Aliyan, M. Moghadam, M. Masoudinia, J. Mol. Catal. A: Chem. 374-375 (2013) 46–52.

[32] Y.M. Liu, W.L. Feng, T.C. Li, H.Y. He, W.L. Dai, W. Huang, Y. Cao, K.N. Fan, J. Catal. 239 (2006) 125–136.

[33] R. Fazael, H. Aliyan, J. Sol-Gel Sci. Tech. 76 (2015) 456-464.

[34] C.T. Kresge, M.E. Leonowicz, W.J. Roth, J.C. Vartuli, J.S. Beck, Nature 359 (1992) 710-712.

[35] M. Che, J.C. Vedrine, Wiley-VCH, Weinheim, Germany 2012.

[36] A. Riga, K. Soutsas, K. Ntampegliotis, V. Karayannis, G. Papapolymerou, Desalination 211 (2007) 72-86.

[37] S. Lathasree, A. Nageswara, B. SivaSankar, V. Sadasivam, K. Rengaraj, J. Mol. Catal. A: Chem. 223 (2004) 101-105.

[38] C.H. Chiou, C.Y. Wu, R.S. Juang, Chem. Eng. J. 139 (2008) 322-329.